ACS SENSORS

Open Access
This article is licensed under CC-BY 4.0

pubs.acs.org/acssensors
Article

Synthetic DNA Transducers Integrate DNA Repair to CRISPR Signal Transduction

Published as part of ACS Sensors special issue "CRISPR in Sensing".

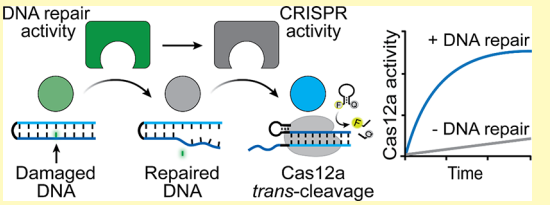
Neda Bagheri, Alessandro Bertucci, Rosa Merlo, and Alessandro Porchetta*

Cite This: *ACS Sens.* 2026, 11, 1634–1644

Read Online

ACCESS | Metrics & More | Article Recommendations | Supporting Information

ABSTRACT: CRISPR-based molecular diagnostics have revolutionized nucleic acid detection, yet the integration of upstream enzyme activity into programmable CRISPR output remains largely unexplored. Here, we present a synthetic transduction platform that directly couples endogenous DNA repair activity with CRISPR-Cas12a activation. By linking base excision repair (BER) events to the structural switching of a programmable DNA transducer, we convert the activity of DNA glycosylases, such as uracil DNA glycosylase (UDG) and human 8-oxoguanine glycosylase (hOGG1), into a robust fluorescence signal via Cas12a-mediated collateral (*trans*-) cleavage. This one-step assay allows rapid and sensitive lysate-based detection of repair activity with high specificity. In addition, it can also be easily adapted to achieve rapid throughput screening of small molecule inhibitors. The rational modular design supports the adaptation to various glycosylase activities, establishing a general framework for transducing DNA repair activity into programmable CRISPR output. Beyond bioanalytical applications, this approach paves the way for the development of synthetic gene circuits that respond to DNA repair activity and CRISPR-based drug screening platforms.



KEYWORDS: *CRISPR, Cas12a, DNA transducer, DNA repair enzyme, inhibitor*

Precise spatiotemporal control of biomolecule interactions at the nanoscale is necessary to advance artificial technologies such as life-like materials,[1,2] artificial cells,[3,4] biosensing,[5,6] and molecular computing.[7,8] Among the molecular frameworks available, DNA nanotechnology offers unparalleled programmability, enabling both static nanoscale scaffolds for the spatial organization of biomolecules[9−11] and dynamic reaction networks capable of input-responsive tasks.[12−18] These systems provide precise temporal control[19] and programmable regulation of downstream biological processes.[20,21] However, despite their versatility, most DNA-based systems remain largely confined to nucleic acid inputs and outputs, facing notable challenges in interfacing with non-nucleic acid molecules and in building efficient ligand-to-oligonucleotide signal transduction networks.[22,23] Additionally, their integration with downstream amplification modules remains challenging, often requiring complex molecular design and suffering from unintended signal leakage.[24]

Advances in synthetic and molecular biology have spawned new tools, such as transcriptional[21,25] and CRISPR[26−32] sensors, that integrate input-responsive DNA systems with downstream enzymatic amplification, allowing the transduction of biological inputs into amplified output. In particular, CRISPR-based platforms harness the collateral (*trans*-) cleavage activity of type V and VI CRISPR effector proteins (e.g. Cas12 and Cas13 enzymes) to achieve high sensitivity through signal amplification.[26,33] Among these, the Cas12a system is activated by recognizing double and single-stranded DNA targets complementary to its CRISPR RNA (crRNA) guide, resulting in a fluorescence output via the non-specific *trans*-cleavage activity of FRET-based DNA reporters.[34,35] Despite the versatility, these systems are limited by the strict requirement of sequence complementarity with the crRNA, which poses challenges for detecting non-nucleic acid targets.[36] To address this limitation, conditional CRISPR-Cas systems regulated by external molecular inputs have been developed, offering promising strategies to partially overcome this limitation.[37−42] Among potential enzyme regulators, the DNA repair machinery, which restores chemically altered DNA (i.e., "DNA damage"), represents a particularly promising system for triggering CRISPR-based responses. DNA repair enzymes act on DNA substrates, which can be rationally designed to become functional CRISPR targets only after enzymatic repair. This strategy offers a novel route to couple DNA repair activity with downstream CRISPR activation, enabling activity-dependent monitoring of DNA repair enzymes. To date, current methods for assessing

Received: November 3, 2025
Revised: January 28, 2026
Accepted: January 30, 2026
Published: February 11, 2026



ACS Publications
© 2026 The Authors. Published by American Chemical Society

https://doi.org/10.1021/acssensors.5c04118
ACS Sens. 2026, 11, 1634–1644

Downloaded from pubs.acs.org/asce/article-pdf/11/2/1634/6486845/se-2025-041187.pdf by guest on 02 September 2026

repair capacity rely largely on indirect approaches, such as measuring gene or protein expression levels or screening for single nucleotide polymorphism (SNP). However, these do not always correlate with actual enzymatic activity, and SNPs can be uninformative when genes are not expressed.[43,44] Cell-based assays like the Comet assay[45] or host cell reactivation[46] (HCR) can assess repair capacity, but often require complex experimental setups to isolate specific repair pathways in cells and tissues. Although DNA repair activity strongly influences the response to DNA-damaging chemotherapeutics,[47] and repair inhibitors have been explored to boost drug efficacy,[48] real-time, direct monitoring tools for specific repair enzymes are still lacking. Chemically modified nucleic acid probes for DNA repair provide a promising alternative,[49] allowing direct visualization of repair in cells[50,51] and compatibility with high-throughput screening of drugs in biological media. However, its clinical utility remains limited by challenges in probe design, synthesis, and relatively high detection thresholds due to the absence of signal amplification.[52] Recently, a few studies have demonstrated direct integration of CRISPR activity with upstream enzymatic activity, including strategies based on enzymatic removal of overhangs (flaps) in split activator designs,[53−55] as well as anti-CRISPR protein-based regulation of Cas12a activity.[56]

Motivated by the above arguments, we report here on a strategy to couple the activity of DNA repair enzymes—typically limited to correcting damaged bases—into a functional trigger for Cas12a-powered signal transduction through a synthetic DNA-based molecular device (hereafter referred to as DNA Transducer, Figure 1). Our approach exploits the high specificity of DNA glycosylases (i.e., UDG and hOGG1), which recognize and excise rationally introduced lesions within the DNA transducer. Repair activity induces a molecular reconfiguration of the DNA transducer that, in turn, activates Cas12a collateral cleavage only after successful repair. By transducing DNA repair into a CRISPR-powered signal output in a one-step assay, we establish a single-step, rapid detection platform capable of real-time monitoring of base excision repair activity directly in cell lysates. Furthermore, we demonstrate that our assay can be readily adapted for the throughput screening of DNA repair enzyme inhibitors.

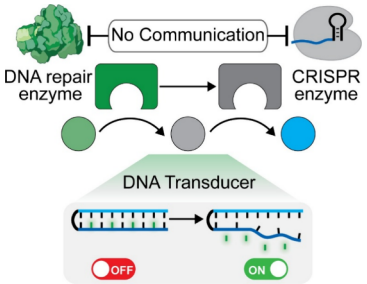


Figure 1. Coupling DNA repair and CRISPR-Cas12a activity using a rationally designed DNA-based molecular transducer. In its native hairpin state, the DNA transducer is the substrate of a DNA repair enzyme, as it contains one or more damaged nucleotides. Although it also presents a CRISPR-targeting sequence in the stem region, it is designed so that CRISPR-Cas12a activity cannot be activated. Once a site-specific BER enzyme exerts its activity on the mutated base(s) of the DNA transducer, the destabilization of the hairpin structure enables the binding of the Cas12a/crRNA (RNP) complex and subsequent Cas12a activation, leading to the generation of a measurable signal.

RESULTS AND DISCUSSION

Synthetic DNA Transducers Enabling DNA Repair-Activated CRISPR Signal Transduction

We have rationally designed a set of synthetic DNA-based molecular transducers (DNA Transducer) that can be programmed to activate the CRISPR-Cas12a system only upon specific repair activity (Figure 1). Our DNA Transducer presents three specific characteristics: (i) it is a synthetic DNA hairpin designed to contain one or more damaged nucleotides in its sequence (indicated by green symbols in Figure 1); (ii) it is recognized as a natural enzymatic substrate of the specific DNA repair enzyme; (iii) it is rationally designed to populate two distinct conformational states, as it adopts a Cas12a-inactive hairpin structure that switches into an Cas12a-active conformation only upon repair activity. Specifically, our design takes advantage of the structural destabilization of the hairpin upon repair activity to effectively regulate the binding and activity of Cas12a ribonucleoprotein (RNP). Previous studies from our group and others have demonstrated that DNA hairpins containing Cas12a target sequences can be rationally engineered to resist Cas12a recognition and cleavage under native conditions.[37,57,58] In particular, we established that Cas12a activity can be regulated by controlling protospacer adjacent motif (PAM) accessibility through structural constraints, where hairpin-to-duplex reconfiguration via target-induced strand displacement effectively enables PAM complementation and Cas12a activation.[37]

In this work, we designed a set of DNA transducers containing base lesions in the nontarget strand (NTS) embedded within the hairpin stem (dark blue sequence in Figure 1). These lesions are specifically targeted by the specific base excision repair (BER) enzyme. Specifically, our system enables the detection of both mono- and bifunctional glycosylases like UDG and hOGG1, respectively. UDG excises uracil to generate abasic (AP) sites, whereas hOGG1 not only excise 8-oxoguanine (Goxo) but also directly introduce nicks. In both cases, the enzymatic processing of the damaged base destabilizes the hairpin structure, enabling Cas12a binding and activation of the *trans*-cleavage activity which results in amplified signal transduction through the digestion of FRET-labelled DNA reporters.

Design of UDG-Responsive DNA Transducers Downstream Controlling Cas12a-Based Activity

As our test bed, we designed the DNA transducer sensitive to uracil DNA glycosylase (UDG) (UDG Transducers, Figure 2) downstream controlling CRISPR-Cas12a system. Uracil (U) is a common DNA damage introduced by dUMP misincorporation or cytosine deamination, resulting in U:A and U:G mispairs, respectively, which can compromise genomic stability,[59] impacting human health.[60,61] The UDG enzyme exhibits specific recognition and excision of uracil bases within DNA by hydrolyzing the N-glycosidic bond (Figure 2A, right panel), generating abasic sites that subsequently initiate the BER pathway. To detect UDG activity, we designed a set of UDG transducers presenting a 20 nt long crRNA targeting portion (blue region, Figure 2B) with different numbers of uracil lesions (green symbols, from 0 to 4 U) in the non-target strand (NTS), embedded within the hairpin stem (dark blue motifs, Figure 2B).

Downloaded from pubs.acs.org/asecf/article-pdf/11/2/1634/6486845/se-2025-041187.pdf by guest on 02 September 2026

https://doi.org/10.1021/acssensors.5c04118
ACS Sens. 2026, 11, 1634−1644

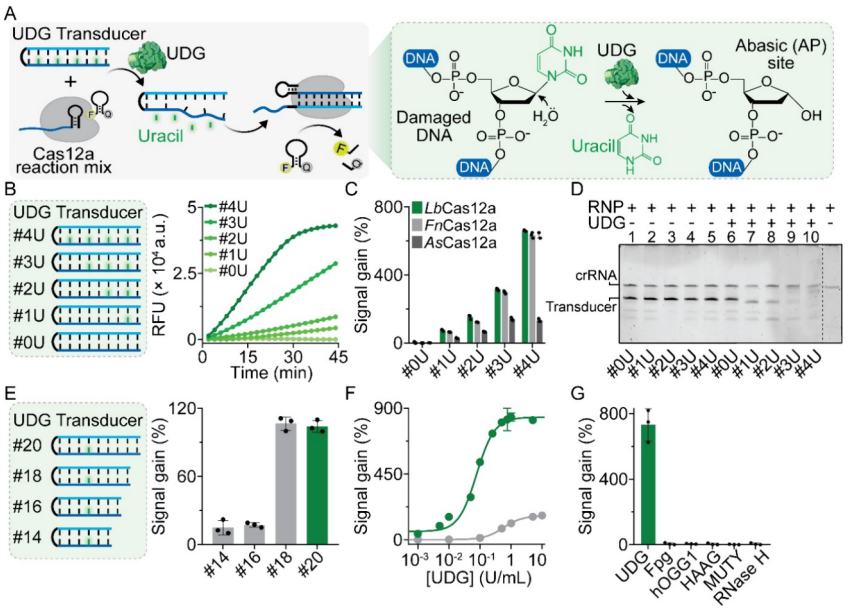


Figure 2. Design and optimization of the UDG transducer triggering Cas12a *trans*-cleavage activity upon hairpin reconfiguration induced by UDG activity. (A) Schematic illustration of our sensing strategy for monitoring UDG activity. The mechanism of excision of the uracil by UDG is indicated on the right side. (B) Fluorescence kinetic analysis over time showing different profiles of collateral cleavage activity of *Lb*Cas12a triggered by different DNA transducers (from #0U to #4U) preincubated with UDG (1 U/mL). Kinetic profiles indicate that *Lb*Cas12a activation depends on the number of uracil bases within the DNA transducer (1 nM). (C) Gain of the fluorescence signal generated by adding UDG (1 U/mL) in a solution containing the DNA transducer #4U (1 nM) using different reaction mixes of Cas12a orthologs. (D) Denaturing PAGE analysis reporting the *cis*-cleavage activity of *Lb*Cas12a in UDG transducers in the absence and presence of UDG (1 U/mL). (E) Gain in fluorescence signal obtained by adding 0.5 U/mL UDG (t = 15 min) using UDG transducers with varying lengths of the crRNA targeting region (from 14 to 20 nt). (F) Dose-response curves of the *Lb*Cas12a-based UDG activity assay (green curve) compared to a direct fluorescent assay (gray curve) using a FRET-labeled UDG transducer (500 nM). (G) Specificity test of the detection platform obtained using saturated concentrations of UDG (0.5 U/mL) and nonspecific enzymes (500 nM MUTY, 10 U/mL for other enzymes). Signal gain (%) was calculated after 15 min of cleavage reaction, representing the relative change in fluorescence signal associated with Cas12a *trans*-cleavage activity upon UDG addition and relative to the background fluorescence obtained in the absence of UDG. The error bars represent the standard deviation from three independent experiments (where they are not visible, they are smaller than the data points).

To investigate Cas12a signal transduction activated by UDG activity, we performed collateral cleavage fluorescence assays by pre-incubation of UDG enzyme (1 U/mL) with different UDG transducers (1 nM) and subsequent addition of a Cas12a reaction mix containing a FRET-based DNA reporter (500 nM) and the Cas12a / crRNA complex (20 nM). As shown in Figure 2B, UDG transducers bearing uracil lesions act as regulatory switches for Cas12a, producing a time-dependent fluorescence increase over time upon UDG addition (1 U/mL). In contrast, the uracil-free control (UDG Transducer #0U) showed no detectable fluorescence change. These results indicate that UDG-mediated uracil excision destabilize the hairpin structure, promoting partial or complete unfolding and thereby enabling Cas12a binding and activation. Increasing the number of uracil within the hairpin from one to four markedly accelerated Cas12a signal transduction, with initial reaction rates (V_0) increasing from 5.6 to 132.7, 489.2, and 1294.5 a.u./min, as determined by linear regression of the initial fluorescence kinetics (Figure 2B). This trend is consistent with increased hairpin destabilization upon generation of multiple abasic sites, which facilitates Cas12a RNP binding and activation. Of note, background fluorescence arising from *trans*-cleavage of unrepaired transducers was independent of uracil content (Figure S1), whereas the signal gain strictly correlated with the number of the uracil lesions, indicating that A-U base pairing does not substantially affect the intrinsic stability of the transducers. To demonstrate the generalizability of our approach, we also tested different Cas12a orthologs of the bacterium *Lachnospiraceae* (*Lb*Cas12a), Francisella novicida (*Fn*Cas12a) and *Acidaminococcus* sp. (*As*Cas1a). All three orthologs show a fluorescence signal gain that increases in response to UDG activity and depends on the number of U within the hairpin stem (Figure 2C). Next, we also studied site-specific (*cis*-)[62] cleavage activity of Cas12a in UDG transducers using denaturing PAGE (Figure 2D). Our results show *cis*-cleavage activity in DNA Transducers containing uracil residues (from UDG Tranducer #1U to #4U) only in the presence of UDG (lanes 7–10, Figure 2D), but not in its absence (lanes 2–5). UDG Transducer #0U remained undigested regardless of UDG treatment (lanes 1 and 6), confirming that repair-induced reconfiguration is required to activate Cas12a.

To further validate the proposed mechanism, we first performed an activity-based fluorescence assay using the same DNA Transducer containing four uracil lesions and terminally labeled with FAM and BHQ1 (UDG Transducer #4U-FQ, 500 nM), enabling direct fluorescence signal transduction. As expected, addition of UDG (10 U/mL) induced a time-dependent fluorescence increase, consistent with uracil excision and consequent hairpin destabilization. In contrast, the corresponding transducer containing four preformed abasic sites (UDG Transducer #4AP-FQ) showed no detectable signal change upon UDG treatment (Figure S2), confirming that

Downloaded from pubs.acs.org/ascef/article-pdf/11/2/1634/6486845/se-2025-041187.pdf by guest on 02 September 2026

https://doi.org/10.1021/acssensors.5c04118
ACS Sens. 2026, 11, 1634−1644

UDG activity is required to trigger structural rearrangement. Thermal denaturation assays further supported this mechanism, revealing a pronounced UDG-dependent destabilization of the hairpin structure, with the melting temperature decreasing from ~85 °C in the absence of UDG to 59.6 °C following enzymatic processing (Figure S3).

To directly assess Cas12a/crRNA binding, we also performed a gel-shift assay using terminally labeled UDG Transducers (#4U-FQ and #4AP-FQ) across a range of Cas12a/crRNA concentrations (0.5−50 nM). The UDG Transducer #4U-FQ remained largely intact, whereas the repaired probe (#4AP-FQ) was efficiently cleaved as Cas12a/crRNA concentration increased, demonstrating that the native hairpin structure restricts Cas12a access and becomes accessible only upon repair (Figure S4). Given that Cas12a collateral activity depends on the length of the double-stranded DNA targeting region, we next evaluated a set of UDG transducers bearing crRNA targeting domains ranging from 14 to 20 nucleotides, each containing a single uracil lesion (Figure 2E). The UDG-induced signal gain (1 U/mL) increased with targeting length, in agreement with previous reports identifying 20-bp duplex regions as optimal for Cas12a activation.[34] Having identified the UDG Transducer #4U as the optimal probe for rapid and sensitive Cas12a signal transduction, we further optimized its concentration to improve the signal-to-noise ratio, as its concentration may affect the background signal, which in turn determines the overall signal change (1 nM, Figure S5). Under optimized experimental conditions, Cas12a-based UDG activity assays achieved a limit of detection (LOD) of 0.0009 U/mL, (RSD 3.4%), with a calibration curve described by the linear equation $F = 250{,}049\ [\mathrm{UDG}] + 8338$ (Figure 2F) at a low concentration range. Comparison with a direct activity-based FRET assay employing the same terminally labelled transducer (DNA Transducer #4U-FQ, 500 nM) highlight a 49.8-fold increase in sensitivity for the Cas12a-based platform ($\mathrm{LOD}_{\#4\mathrm{U\text{-}FQ}}$ = 0.02 U/mL, $F = 5031\ [\mathrm{UDG}] + 3236$). Although several CRISPR-Cas12-based strategies for UDG activity detection report even lower detection limits,[63−65] they generally rely on multiple auxiliary enzymes (e.g., DNA ligase, nicking enzyme, Endonuclease IV, polymerase, AP-lyase), complex probe designs and multistep reactions workflows (e.g., ligation, polymerization), which can compromise scalability, throughput, and a simple mix-and-read format (Table 1). In contrast, our platform achieves a balance between high sensitivity and simplicity, offering a straightforward, single-step approach suitable for rapid and scalable UDG detection. The platform exhibits also high specificity, as no significant signal variation is observed in the presence of nonspecific enzymes (Figure 2G). Finally, applicability to human single-strand selective monofunctional uracil DNA glycosylase (hSMUG1) further demonstrates the robustness and versatility of the platform (Figure S6).

Cas12a-Based Real-Time Monitoring of UDG Activity in Human Cell Lysate

Motivated by the above results, we tested our Cas12a-based UDG activity assay on wild-type HEK293T cell lysate (Figure 3A) by adding UDG. Our assay can detect UDG activity in HEK293T cell lysate in the dynamic range of 0.0085 to 0.65 U/mL ($K_{1/2} = 0.07 \pm 0.01$ U/mL, Figure 3B) with a linear response described by $F = 366{,}872\ [\mathrm{UDG}] + 7522$ and a LOD of 0.0009 U/mL calculated after 15 min of reaction (Figure S7). To evaluate the accuracy of the Cas12a-based method, we performed recovery tests by spiking UDG at four different concentrations into HEK293T cell lysate, confirming that our approach can be used to detect its activity in complex biological samples (Figure 3C). Control experiments in wild-type HEK293T lysate were also performed in the presence and absence of UNG inhibitor (UGI), highlighting that endogenous UDG activity cannot be detected by our Cas12a-based system (Figure S8). Additionally, we assessed the stability over time of the UDG transducer #4U in HEK293T lysate through PAGE analysis which showed no detectable degradation compared with buffer conditions (Figure S9). Then, to demonstrate real-time monitoring of UDG activity, we used HEK293T lysate with overexpressed uracil-N-glycosylase (UNG) activity. UNG is a Family I member of the UDG superfamily, which is composed of six distinct subfamilies of uracil-excising enzymes.[71] To do so, a subsequent dilution of HEK293T lysate was tested by simply adding the Cas12a reaction mix with the UDG transducer #4U, which confirmed highly sensitive detection (Figure 3D). To further confirm that the Cas12a reaction network is triggered exclusively by UNG activity in cell lysate, we

Table 1. An Overview of Recently Reported CRISPR Methods for the Detection of UDG and hOGG1

LOD (U/mL)	linear/dynamic range (U/mL)	analysis time	auxiliary enzymes	single step	amplification	ref
0.00061 (UDG) and 0.09 (hOGG1)	0.0012−0.019 (UDG) and 0.1−1 (hOGG1)	>1h		no		66
0.0018	0−0.125	50 min		no		67
0.00081 (UDG) and 26.66 (hOGG1)	0.0078−0.125 (UDG) and 125−2000 (hOGG1)	>50 min	Exo I & III	no		68
0.005	0.005−5	>1h		no		54
	0.0001−0.0125	~2h	Endo IV, Bst. DNA polymerase, Nt.BstNBI nickase	no	isothermal exponential amplification reaction (EXPAR)	69
2.5×10^{-6}		~100 min	Endo IV	no		65
3.1×10^{-5}	5.0×10^{-5}−0.1	3.5 h	Endo IV, Klenow fragment DNA polymerase, Nt.BbvCI nickase	no	enhanced strand displacement amplification (ESDA)	63
5×10^{-6}	2×10^{-5}−2×10^{-3}	>3 h	Endo IV, terminal transferase (TdT)	no	terminal deoxynucleotidyl transferase (TdT)-catalyzed substrate extension	64
3.7×10^{-4}	0.0001−0.25	>4 h	T4 DNA ligase, proteinase K	no		70
0.0009 (UDG) and 14.8 ng/mL (hOGG1)	0.009−0.7 (UDG) and hOGG1 41.2−3339 ng/mL (hOGG1)	<40 min		yes		this work

Downloaded from pubs.acs.org/ascef/article-pdf/11/2/1634/6486845/se-2025-041187.pdf by guest on 02 September 2026

https://doi.org/10.1021/acssensors.5c04118
ACS Sens. 2026, 11, 1634−1644

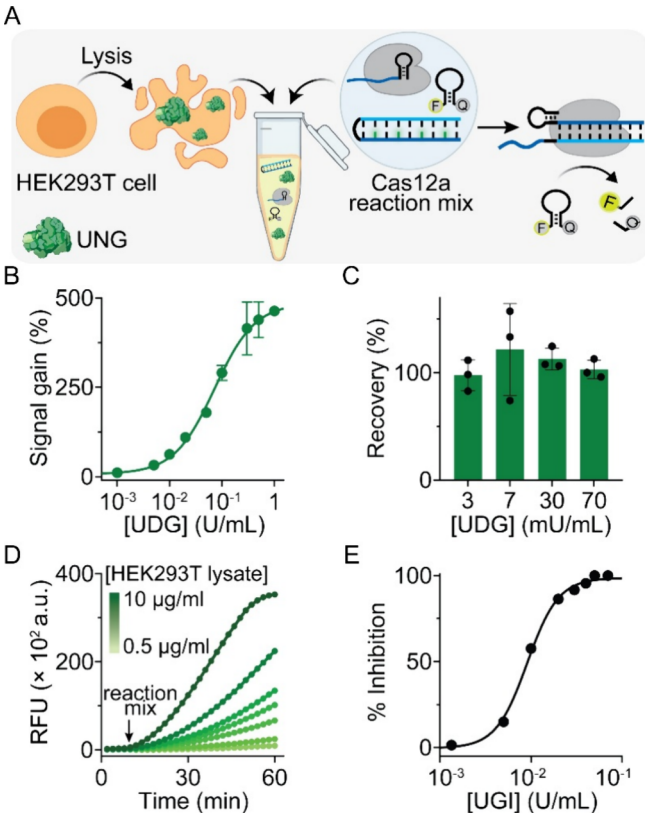


Figure 3. Cas12-based UDG/UNG activity assay in human HEK293T lysate. (A) Schematic illustration of the Cas12a-based reaction network for monitoring UNG activity in human HEK293T cells. (B) Calibration curve of the dose-response of UDG activity in human HEK293T cells obtained using the optimized Cas12a-based reaction mix (DNA transducer #4U 1 nM, Cas12a-crRNA 20 nM, and DNA reporter based on FRET 500 nM). (C) Recovery test in HEK293T cell lysate achieved by spiking with various concentrations of UDG. (D) Fluorescence kinetic traces of collateral activity of Cas12a in human HEK293T cell lysate overexpressing UNG. (E) UNG activity inhibition plot using HEK293T cell lysates overexpressing UNG and the Cas12a reaction mix (DNA transducer #4U 1 nM, Cas12a-crRNA 20 nM, and FRET-based DNA reporter 500 nM) in the presence of varying concentrations of the UGI inhibitor. Recovery and inhibition tests were conducted according to the experimental procedures reported in the Supporting Information. Error bars represent the standard deviation from three independent experiments (where they are not visible, they are smaller than the data points).

conducted a control experiment in the presence of the uracil-DNA glycosylase inhibitor (UGI). UGI specifically inhibits UNG by forming a stable, irreversible UNG: UGI protein complex in a 1:1 stoichiometry, thus preventing UNG from excising uracil from DNA.[71] As expected, by increasing UGI concentrations in cell lysate (10 μg/mL), a dose-dependent reduction in fluorescence intensity is observed (Figure 3E). These results indicate the capacity of the assay to enable real-time monitoring of glycosylase activity and also screening of inhibitors directly in cell lysate.

Synthetic DNA Transducers Rewire hOGG1 Activity into Cas12a Signal Amplification

Our strategy is highly versatile, as it enables monitoring of various classes of glycosylases by simply changing the specific DNA damage within the DNA transducer. As a proof-of-concept demonstration, we tested human 8-oxoguanine DNA glycosylase 1 (hOGG1), which is a bifunctional glycosylase that not only excises damaged bases but also successively cleaves phosphodiester bonds at the generated abasic sites.[72] hOGG1 is a key enzyme involved in repairing oxidative DNA damage that specifically detects 8-oxoguanine (8-oxoG), an oxidative DNA lesion that can cause transversion mutations if unrepaired.[73,74] Given the central role of oxidative DNA damage in the development of cancer,[75,76] neurodegenerative diseases,[77] and aging,[78] monitoring OGG1 activity could provide valuable information about these conditions and their progression. Here, we designed an hOGG1-responsive DNA transducer that preserves the same Cas12a targeting region used for UDG monitoring, while incorporating a single 8-oxoG lesion in the middle of the crRNA targeting sequence (red symbol, Figure 4A). This design allows the same Cas12a reaction mix to be used for both UDG and hOGG1 sensing, directly demonstrating the generalizability of the platform. Upon hOGG1-mediated excision of 8-oxoG from the molecular transducer, the enzyme's associated lyase activity induces strand nicking, leading to the release of a short DNA fragment (9 nt) from the hairpin stem. This event destabilizes the hairpin architecture, exposing unpaired nucleotides within the target strand and thereby enabling Cas12a RNP binding, activation, and subsequent trans-cleavage of the fluorescent reporter (Figure 4A). Our assay was initially validated using E. coli formamidopyrimidine-DNA glycosylase (Fpg), a bacterial analogue of hOGG1.[79] Although both enzymes initiate DNA cleavage through β-elimination to remove the 3'-oxygen from the phosphate of the AP site, Fpg uniquely performs an additional δ-elimination step, also removing the 5'-oxygen.[83] Melting temperature analysis of the

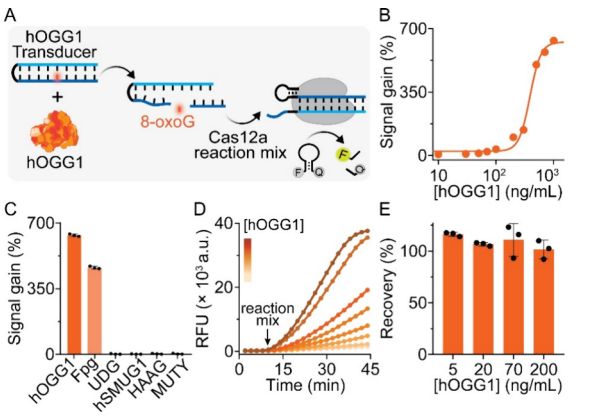


Figure 4. Cas12a-powered activity assay for monitoring hOGG1 activity. (A) Scheme of our detection strategy based on an 8 oxoG-containing DNA transducer (hOGG1 transducer) that triggers Cas12a-based signal transduction during repair activity. (B) Calibration curve obtained using the hOGG1 transducer (1 nM) by adding increasing concentrations of hOGG1 and the Cas12 reaction mix. (C) Specificity test in the presence of nonspecific enzymes (MUTY 500 nM, other enzymes 10 U/mL). (D) Fluorescence kinetic traces of Cas12a activation in HEK293T cell lysate supplemented with increasing concentrations (3, 10, 30, 50, 100, 150, 300, and 500 ng/mL) of hOGG1. (E) Recovery test in HEK293T cell lysate spiked with different concentrations of hOGG1. Recovery tests were conducted according to the experimental procedures reported in the Supporting Information. Error bars represent the standard deviation from three independent experiments (where they are not visible, they are smaller than the data points).

Downloaded from pubs.acs.org/ascef/article-pdf/11/2/1634/6486845/se-2025-041187.pdf by guest on 02 September 2026

https://doi.org/10.1021/acssensors.5c04118
ACS Sens. 2026, 11, 1634−1644

hOGG1 transducer revealed a substantial decrease from ~82.4 °C prior to enzymatic treatment to ~40.6 °C following Fpg activity (Figure S10), quantitatively confirming that nicking induces significant hairpin destabilization. Denaturing PAGE further demonstrated that the *cis*-cleavage activity of Cas12a occurs exclusively for the DNA transducer containing the 8-oxoG lesion after Fpg-mediated repair (lane 4, Figure S11). In contrast, the DNA Transducer lacking the 8-oxoG lesion (i.e., hOGG1 Transducer without Goxo) remains undigested even in the presence of Fpg (Lanes 5–8). Our Cas12a-based Fpg activity assay exhibits high sensitivity with a limit of detection (LOD) of 0.001 U/mL for Fpg, outperforming direct activity-based assays (LOD = 0.3 U/mL) under the same conditions (Figure S12). We then applied our CRISPR platform to hOGG1 detection, achieving sensitive detection with a LOD of 14.2 ng/mL and a linear calibration curve described by $F = 34.95\ [\text{hOGG1}] + 5520$, Figure 4B), together with high specificity against nonspecific enzymes (Figure 4C). Our CRISPR-based platform was further assessed in human HEK293T cell lysates by spike and recovery assays by adding known concentrations of hOGG1 (Figure 4D), following the dose-response fluorescence kinetics over time. Statistical analysis revealed a linear detection range of 3 to 300 ng/mL ($F = 103.9\ [\text{hOGG1}] + 11{,}497$), with an R^2 value of 0.995 (Figure S13). Furthermore, we assessed the recovery percentages of spiked hOGG1 at four different concentrations, achieving recovery rates ranging from 101% to 115% (Figure 4E), confirming the accuracy of our single-step detection method. Additional tests in HEK293T lysate with and without an hOGG1 inhibitor showed no measurable contribution from endogenous hOGG1, indicating that background fluorescence arises from the transducer itself rather than endogenous enzyme activity (Figure S14).

Cas12a-Based Throughput Screening of hOGG1 Inhibitors

Recent studies indicated that inhibition of hOGG1 is a promising strategy for developing treatments for cancer and inflammation.[80,81] Taking advantage of the high sensitivity and rapid response of our single-step CRISPR-based hOGG1 activity assay, we readapted our system for the throughput screening of small molecule inhibitors (Figure 5A). To this end, we tested several well-characterized small-molecule inhibitors targeting hOGG1 and Fpg. Specifically, we evaluated two inhibitors of hOGG1 that operate through different mechanisms. Indeed, O8 (Inh #1) prevents the catalytic AP lyase activity of hOGG1 without affecting protein-substrate binding,[82] while SU0268 (Inh #2) inhibits both DNA binding and base excision activity of the enzyme.[83] Furthermore, we examined three derivatives of 2-thioxanthine (2TX) (Inh #3, #4, and #5), known addition, PAGE analysis of the hOto irreversibly inhibit zinc finger (ZnF)-containing Fpg/Nei DNA glycosylases.[84,85] We tested a range of inhibitor concentrations (0.1 μM to 350 μM) to assess the inhibition of hOGG1 and Fpg. Consistent with previous studies,[82,83] hOGG1 inhibition exhibits a selective dependence on Inh #1 (O8) and Inh #2 (SU0268), producing IC50 values of 2.5 ± 0.5 μM and 28.6 ± 7.3 μM, respectively (Figure 5B). On the contrary, Inh #3 and Inh #5 selectively inhibit Fpg (Figure S15). On the other hand, Inh #4 shows dual inhibition, affecting both hOGG1 (IC50 = 11.9 ± 0.4 μM) and Fpg (IC50 = 70.3 ± 0.7 μM) (Figure 5B and Figure S9). The heatmap reported in Figure 5C offers a concise overview of the inhibition effects at a fixed concentration of 200 μM, highlighting the different activity between the bacterial and human enzymes, and confirms the selective inhibition profiles of each inhibitor. Furthermore, it confirms that our Cas12a-based screening can be used to distinguish between various inhibitors based on their target specificity. As a control, we confirmed that Cas12a activity is not affected by the presence of 10% DMSO-which is required for inhibitor solubilization – and the Cas12a signal off is exclusively due to glycosylase inhibition (Figures S16 and S17). In addition, PAGE analysis of the hOGG1 Transducer incubated in 10% DMSO showed no detectable difference in band integrity, indicating that this experimental condition does not affect nucleic acid stability (Figure S18). It is important to note that single-step CRISPR-based screening is performed in a 96-well plate microvolume (25 ul) and takes approximately 15 min after RNP addition. It costs approximately less than 0.7 euros per test, as it requires a minimal amount of DNA Transducer (1 nM) and Cas12a reaction mix (20 nM RNP and 500 nM FRET-based DNA reporter), due to the sensitive nature of the assay. The assay yielded a Z′ factor of 0.82, which confirms its robustness and compatibility with high-throughput screening applications.

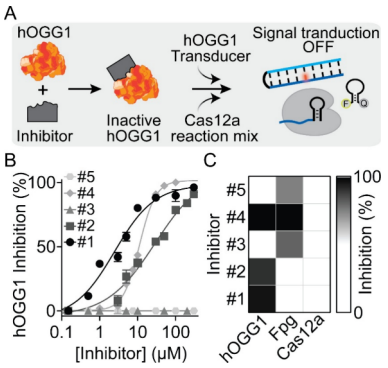


Figure 5. Cas12a-based throughput screening of hOGG1 inhibitors. (A) Schematic description of the test. (B) Plot of inhibition of hOGG1 (%) activity at various concentrations of different inhibitors. (C) Heatmap showing % inhibition observed with different inhibitors (200 μM) on hOGG1, Fpg, and Cas12a/crRNA complex (20 nM), as a control experiment. In (B) and (C), Inh #1–#5 represent O8, SU0268, 2-thioxanthine, mercapto-6,8-purinediol, and 8-mercaptoadenine, respectively. Experiments were carried out at 37 °C by adding the Cas12a reaction mix (500 nM of FRET-based DNA reporter and 20 nM of the Cas12a/crRNA complex) to a 25 μL buffer solution (10 mM Tris-HCl, 50 mM NaCl, 10 mM $MgCl_2$, and 0.1 mg/mL of BSA, at pH 7.9) containing the hOGG1 transducer (1 nM), hOGG1 (700 ng/mL), and varying concentrations of inhibitors. Inhibition (%) for each inhibitor was calculated after a 15-min cleavage reaction, as described in the Experimental Section (Data Analysis). Error bars represent the standard deviation from three independent experiments (where they are not visible, they are smaller than the data points).

■ CONCLUSIONS

In this study, we develop synthetic DNA transducers that activate CRISPR-Cas12a after enzymatic repair, allowing for rapid

Downloaded from pubs.acs.org/acsef/article-pdf/11/2/1634/6486845/se-2025-041187.pdf by guest on 02 September 2026

https://doi.org/10.1021/acssensors.5c04118
ACS Sens. 2026, 11, 1634–1644

and real-time monitoring of DNA glycosylase activity. Using the substrate specificity of repair enzymes for damaged DNA bases, we show that glycosylase activity can trigger Cas12a-mediated signal transduction, effectively converting DNA damage recognition into amplified fluorescence output. This one-step assay couples lesion excision with Cas12a *trans*-cleavage to achieve sensitive detection of glycosylase activity directly in complex biological samples such as cell lysates.

Our platform addresses key limitations of conventional activity-based assays, including reliance on chemically modified (unnatural) DNA probes, low sensitivity, and multistep workflows. In contrast to previously reported CRISPR-based strategies, our system operates without auxiliary enzymes, complex probe architectures, or sequential reagent additions, as signal amplification is achieved by simply mixing of components in solution Table 1. The assay is based on DNA hairpins substrates that closely mimic the natural targets for the DNA repair enzymes, and its simple design enables straightforward adaptation to different DNA lesions (e.g., uracil or 8-oxoG), supporting broad applicability across DNA repair pathways. Beyond bioanalytical applications, the platform provides a robust framework for throughput screening of DNA repair inhibitors, as demonstrated here using representative small molecule inhibitors of hOGG1 and Fpg. We demonstrate this by evaluating several small molecule inhibitors of hOGG1 and Fpg. More broadly, this approach facilitates mechanistic studies of DNA repair and offer opportunity for integration into synthetic gene circuits responsive to cellular states, as well as for real-time monitoring of DNA repair in real time and drug screening.

EXPERIMENTAL SECTION

Reagents and Materials

Sodium chloride (NaCl), sodium hydroxide (NaOH), magnesium chloride ($MgCl_2$), Trizma hydrochloride (Tris−HCl), Trizma, boric acid, ethylenediamine tetraacetic acid (EDTA), acrylamide/bis-acrylamide 40% solution, ethylenediamine tetraacetic acid (EDTA), *N*,*N*,*N*′,*N*′-tetramethyl ethylenediamine (TEMED), ammonium persulfate (APS), DEPC-treated water, bovine serum albumin (BSA), 2-mercapto-6,8-purinediol, 8-mercaptoadenine, Dimethyl Sulfoxide (DMSO). 2-thioxanthine and Gel Loading Buffer II were purchased from ThrmoFisher Scientific. Invitrogen provided SYBR Gold nucleic acid stain. OGG1 inhibitors O8 and SU0268 were purchased from MedChemExpress. Uracil DNA glycosylase (UDG), uracil glycosylase inhibitor (UGI), E. coli formamidopyrimidine DNA glycosylase (Fpg), human single-strand selective monofunctional uracil-DNA glycosylase 1 (hSMUG1) and EnGen Lba Cas12a from *Lachnospiraceae* bacterium ND2006 were purchased from New England Biolabs (Beverly, MA, USA). *As*Cas12a from *Acidaminococcus* sp. was sourced from Integrated DNA Technologies (IDT). *Fn*Cas12a from Francisella novocida bacterium was generously provided by the laboratory of Professor Giuseppe Perugino at the University of Naples "Federico II" which was produced as previously reported in our work.[42] Human 8-oxoguanine DNA glycosylase (OGG1), transient overexpression lysate of uracil-DNA glycosylase (UNG), and HEK293T cell lysate were purchased from Origene. The enzymes were aliquoted and stored at −20 °C or −80 °C.

Oligonucleotides

All the oligonucleotides employed in this work were synthesized, labeled, and HPLC-purified by Metabion International AG (Planegg, Germany) and used without further purification. DNA and RNA oligonucleotides were dissolved to 100 μM in 100 mM Tris-Hcl pH 7.5, and DEPC-treated water, respectively. All oligonucleotides were aliquoted and stored at −20 °C until use. The final concentration of the oligonucleotides was confirmed using Thermo Scientific Multiskan SkyHigh Microplate Spectrophotometer.

Fluorescence Experiments

Fluorescence kinetic measurements were performed in a 25 μl buffer solution containing 10 mM Tris-HCl, 50 mM NaCl, 10 mM $MgCl_2$, and 0.1 mg/mL BSA, at pH 7.9 unless otherwise specified. The measurements were carried out using a Stratagene Mx3005P Real-Time PCR System (Agilent Technologies, Santa Clara, CA) with 96-well PCR plates and optically transparent caps (Thermo Scientific). The fluorescence signals were recorded every 2 min, starting from the initial 2-min time point, at a constant temperature of 37 °C using a filter set optimized for FAM detection. For fluorescence melting assays, a 1 mL cuvette and a JASCO PF-8050 spectrofluorometer with excitation wavelength set at 490 (±5) nm and acquisition at 520 (±5) nm were used. Detailed procedures employed in the different experiments are reported in the Supporting Information.

Fluorescence activity assays (e.g. direct assay without CRISPR amplification) were conducted by adding varying concentrations of UDG or Fpg to a buffer solution (10 mM Tris-HCl, 50 mM NaCl, 10 mM $MgCl_2$, 0.1 mg/mL BSA, pH 7.9) containing FRET-labeled UDG (#4U-FQ, 500 nM) or hOGG1 DNA Transducer (#4U-FQ, 500 nM), respectively. An aliquot of 25 μl of the mixture was then transferred to a 96-well PCR plate, and fluorescence intensity was monitored. Data plotted represents the intensity of fluorescence at the equilibrium.

Fluorescence *Trans*-Cleavage Assays for UDG and hOGG1 Detection

Fluorescence *trans*-cleavage experiments for UDG or hOGG1 detection were conducted by adding a concentration of target enzyme to the buffer solution (10 mM Tris-HCl, 50 mM NaCl, 10 mM $MgCl_2$ 0.1 mg/mL BSA, pH 7.9) containing 1 nM UDG DNA Transducer or hOGG1 DNA Transducer, respectively, and 500 nM FRET-based DNA reporter. An aliquot of 22.5 μl of this mixture was transferred to the 96-well PCR plate, followed by the addition of 2.5 μl of the Cas12a/crRNA (RNP) complex, which had been pre-incubated at 37 °C for 30 min with 200 nM of both Cas12a and crRNA, achieving a final concentration of 20 nM. Fluorescence intensity was then immediately monitored over time.

Data Analysis

Signal gain (%) is calculated at 15 min from the addition of the RNP complex to the reaction mixture unless otherwise stated. It represents the relative fluorescence signal change upon the addition of the target, relative to the background fluorescence obtained in the presence of the DNA Transducer. The signal gain is calculated using the following formula:

$$\text{signal gain } (\%) = \frac{F_{\text{target}} - F_0}{F_0} \times 100$$

where F_{target} is the fluorescence signal measured upon addition of the target enzyme and F_0 is the fluorescence signal generated by the DNA Transducer in the absence of the target enzyme, respectively. Plots of signal gain (%) vs concentration of target enzyme were fitted with the following four parameters logistic equation:

$$\text{signal gain } (\%) = B_{\min} + (B_{\max} - B_{\min}) \frac{[\text{target enzyme}]^{n_H}}{K_{\frac{1}{2}}^{n_H} + [\text{target enzyme}]^{n_H}}$$

Where $B_{\min}$ and $B_{\max}$ are the minimum and maximum signal gain (%) values, respectively; $K_{1/2}$ is the concentration of the target at a half-maximum signal gain (%), [target enzyme] is the concentration of the target enzyme, and n_H is the Hill coefficient. The limit

Downloaded from pubs.acs.org/ascef/article-pdf/11/2/1634/6486845/4/se-2025-041187.pdf by guest on 02 September 2026

https://doi.org/10.1021/acssensors.5c04118
ACS Sens. 2026, 11, 1634−1644

of detection (LOD) was calculated based on the ratio of 3 times of standard deviation of the blank to the slope of linear regression at a low concentration range.[86] All Statistical analyses were completed using GraphPad Prism 8.0.

The inhibition percentage for different inhibitors was calculated as follows:

$$\text{inhibition } (\%) = 1 - \frac{F_{inh} - F_{hOGG1\ transducer}}{F_{hOGG1\ transducer,enzyme} - F_{hOGG1\ transducer}} \times 100$$

Where F_{inh} is the fluorescence signal of the hOGG1 DNA Transducer measured after the preincubation with different concentrations of inhibitors and hOGG1 (ng/mL) or Fpg (U/mL), $F_{hOGG1\ transducer;enzyme}$ represents the fluorescence signal of the hOGG1 DNA Transducer in the presence of hOGG1 (ng/mL) or Fpg (U/mL). In contrast, $F_{hOGG1\ transducer}$ denotes the fluorescence signal in the absence of hOGG1 or Fpg. IC50 values were calculated using GraphPad Prism 8.0 software with a four-parameter logistic dose-response curve.

Z'-factor was determined as follows:

$$Z' = 1 - \frac{3(\sigma_{inh} + \sigma_{Fpg})}{|F_{inh} - F_{Fpg}|}$$

Where F_{inh} is the fluorescence signal of the hOGG1 DNA Transducer measured after the preincubation with Mercapto-6,8-purinediol inhibitor (150 μM) and Fpg (0.75 U/mL) and F_{Fpg} represents the fluorescence signal of the hOGG1 DNA Transducer in the presence of Fpg (0.75 U/mL). Row A and B of the 96-well plate were used to determine F_{inh} and F_{Fpg}, respectively and where σ_{inh} and σ_{Fpg} represent the standard deviations of the two groups.

■ ASSOCIATED CONTENT

Supporting Information

The Supporting Information is available free of charge at https://pubs.acs.org/doi/10.1021/acssensors.5c04118.

Additional experimental details, oligonucleotides sequences, and methods, including supporting figures (DOCX)

■ AUTHOR INFORMATION

Corresponding Author

Alessandro Porchetta – *Department of Chemical Science and Technologies, University of Rome, Tor Vergata, Via della Ricerca Scientifica 1, Rome 00133, Italy; Biostructures and Biosystems National Institute (INBB), Via dei Carpegna 19, Rome 00165, Italy;* orcid.org/0000-0002-4061-5574; Email: alessandro.porchetta@uniroma2.it

Authors

Neda Bagheri – *Department of Chemical Science and Technologies, University of Rome, Tor Vergata, Via della Ricerca Scientifica 1, Rome 00133, Italy;* orcid.org/0009-0005-0805-8201

Alessandro Bertucci – *Department of Chemistry, Life Sciences, and Environmental Sustainability, University of Parma, Parco Area Delle Scienze 17/A, Parma 43124, Italy; Biostructures and Biosystems National Institute (INBB), Via dei Carpegna 19, Rome 00165, Italy;* orcid.org/0000-0003-4842-9909

Rosa Merlo – *Institute of Biosciences and BioResources, National Research Council of Italy, Via Pietro Castellino 111, Naples 80131, Italy;* orcid.org/0000-0001-8400-193X

Complete contact information is available at: https://pubs.acs.org/10.1021/acssensors.5c04118

Author Contributions

All authors have approved the final version of the manuscript. N.B. conceived, designed, and performed experimental work, analyzed data, and wrote the first draft. A.B. and R.M. analyzed the data and wrote the manuscript. A.P. conceived the idea, supervised the experimental activities, and wrote the manuscript.

Notes

The authors declare no competing financial interest.

■ ACKNOWLEDGMENTS

The research leading to these results has received funding from AIRC under MFAG 2022 - ID. 27151 project - Pi. Porchetta Alessandro. AP and AB acknowledges financial support under the National Recovery and Resilience Plan (NRRP), Mission 4, Component 2, Investment 1.1, Call for tender No. 104 published on 2.2.2022 by the Italian Ministry of University and Research (MUR), funded by the European Union - NextGenerationEU - Project Title "CRISPR-Cas-based sensing platforms for the monitoring of clinically relevant antibodies" - CUP D53D23009090001- Project Code 2022FPYZ2N - Grant Assignment Decree No. 958 adopted on 30-06-2023 by the Italian Ministry of Ministry of University and Research (MUR) and by 'PNRR M4C2-Investimento 1.4- CN00000041' financed by NextGenerationEU. N.B. was supported by a Fondazione Umberto Veronesi postdoctoral fellowship.

■ REFERENCES

(1) Buddingh', B. C.; van Hest, J. C. M. Artificial Cells: Synthetic Compartments with Life-like Functionality and Adaptivity. *Acc. Chem. Res.* **2017**, *50* (4), 769–777.

(2) Seo, H.; Lee, H. Programmable Enzymatic Reaction Network in Artificial Cell-Like Polymersomes. *Adv. Sci.* **2024**, *11* (24), No. 2305760.

(3) Qiao, Y.; Li, M.; Qiu, D.; Mann, S. Response-Retaliation Behavior in Synthetic Protocell Communities. *Angew. Chem., Int. Ed.* **2019**, *131* (49), 17922–17927.

(4) Buddingh', B. C.; Elzinga, J.; van Hest, J. C. Intercellular communication between artificial cells by allosteric amplification of a molecular signal. *Nat. Commun.* **2020**, *11* (1), 1652.

(5) Wang, C.; Han, C.; Du, X.; Guo, W. Versatile CRISPR-Cas12a-Based Biosensing Platform Modulated with Programmable Entropy-Driven Dynamic DNA Networks. *Anal. Chem.* **2021**, *93* (38), 12881–12888.

(6) Khumngern, S.; Jeerapan, I. Synergistic Convergence of Materials and Enzymes for Biosensing and Self-Sustaining Energy Devices towards on-Body Health Monitoring. *Commun. Mater.* **2024**, *5* (1), 135.

(7) Katz, E. Enzyme-Based Logic Gates and Networks with Output Signals Analyzed by Various Methods. *ChemPhysChem* **2017**, *18* (13), 1688–1713.

(8) Ivanov, N. M.; Baltussen, M. G.; Regueiro, C. L. F.; Derks, M. T. G. M.; Huck, W. T. S. Computing Arithmetic Functions Using Immobilised Enzymatic Reaction Networks. *Angew. Chem., Int. Ed.* **2023**, *135* (7), No. e202215759.

(9) Bugada, L. F.; Smith, M. R.; Wen, F. Engineering Spatially Organized Multienzyme Assemblies for Complex Chemical Transformation. *ACS Catal.* **2018**, *8* (9), 7898–7906.

(10) Zhang, P.; Liu, X.; Liu, P.; Wang, F.; Ariyama, H.; Ando, T.; Lin, J.; Wang, L.; Hu, J.; Li, B.; Fan, C. Capturing Transient Antibody

Downloaded from pubs.acs.org/asce/article-pdf/11/2/1634/6486845/se-2025-041187.pdf by guest on 02 September 2026

Conformations with DNA Origami Epitopes. *Nat. Commun.* **2020**, *11* (1), 3114.
(11) Praetorius, F.; Dietz, H. Self-assembly of genetically encoded DNA-protein hybrid nanoscale shapes. *Science* **2017**, *355* (6331), No. eaam5488.
(12) Yue, L.; Wang, S.; Zhou, Z.; Willner, I. Nucleic Acid Based Constitutional Dynamic Networks: From Basic Principles to Applications. *J. Am. Chem. Soc.* **2020**, *142* (52), 21577–21594.
(13) Zhang, D. Y.; Seelig, G. Dynamic DNA nanotechnology using strand-displacement reactions. *Nat. Chem.* **2011**, *3* (2), 103–113.
(14) Farag, N.; Đorđević, M.; Del Grosso, E.; Ricci, F. Dynamic and Reversible Decoration of DNA-Based Scaffolds. *Adv. Mater.* **2023**, *35* (18), No. 2211274.
(15) Grossi, G.; Dalgaard Ebbesen Jepsen, M.; Kjems, J.; Andersen, E. S. Control of enzyme reactions by a reconfigurable DNA nanovault. *Nat. Commun.* **2017**, *8* (1), 992.
(16) Simmel, F. C.; Yurke, B.; Singh, H. R. Principles and Applications of Nucleic Acid Strand Displacement Reactions. *Chem. Rev.* **2019**, *119* (10), 6326–6369.
(17) Bertucci, A.; Porchetta, A.; Del Grosso, E.; Patiño, T.; Idili, A.; Ricci, F. Protein-Controlled Actuation of Dynamic Nucleic Acid Networks by Using Synthetic DNA Translators. *Angew. Chem., Int. Ed.* **2020**, *59* (46), 20577–20581.
(18) Ranallo, S.; Sorrentino, D.; Delibato, E.; Ercolani, G.; Plaxco, K. W.; Ricci, F. Protein−Protein Communication Mediated by an Antibody-Responsive DNA Nanodevice. *Angew. Chem., Int. Ed.* **2022**, *61* (12), No. e202115680.
(19) Bucci, J.; Irmisch, P.; Del Grosso, E.; Seidel, R.; Ricci, F. Orthogonal enzyme-driven timers for DNA strand displacement reactions. *J. Am. Chem. Soc.* **2022**, *144* (43), 19791–19798.
(20) Sorrentino, D.; Ranallo, S.; Nakamura, E.; Franco, E.; Ricci, F. Synthetic Genes For Dynamic Regulation Of DNA-Based Receptors. *Angew. Chem., Int. Ed.* **2024**, *63* (17), No. e202319382.
(21) Shi, X.; Hu, C.; Guo, B.; Zhang, C.; Xue, Y.; Yang, Z.; Wang, F. Programmable Transcriptional−Translation Active Sensors for miRNA-Responsive Gene Imaging and Theranostics in Mammalians. *ACS Sens.* **2025**, *10* (6), 4646–4657.
(22) Zhang, Q.-L.; Wang, L.-L.; Liu, Y.; Lin, J.; Xu, L. A Kinetically Controlled Platform for Ligand-Oligonucleotide Transduction. *Nat. Commun.* **2021**, *12* (1), 4654.
(23) Takezawa, Y.; Mori, K.; Huang, W.-E.; Nishiyama, K.; Xing, T.; Nakama, T.; Shionoya, M. Metal-Mediated DNA Strand Displacement and Molecular Device Operations Based on Base-Pair Switching of 5-Hydroxyuracil Nucleobases. *Nat. Commun.* **2023**, *14* (1), 4759.
(24) Li, J.; Li, T.; Zou, Z.; Li, H.-W. The Trend of Nonenzymatic Nucleic Acid Amplification: Strategies and Diagnostic Application. *Precis. Chem.* **2025**, *3* (4), 187–205.
(25) Jung, J. K.; Alam, K. K.; Verosloff, M. S.; Capdevila, D. A.; Desmau, M.; Clauer, P. R.; Lee, J. W.; Nguyen, P. Q.; Pastén, P. A.; Matiasek, S. J.; Gaillard, J.-F.; Giedroc, D. P.; Collins, J. J.; Lucks, J. B. Cell-Free Biosensors for Rapid Detection of Water Contaminants. *Nat. Biotechnol.* **2020**, *38* (12), 1451–1459.
(26) Kaminski, M. M.; Abudayyeh, O. O.; Gootenberg, J. S.; Zhang, F.; Collins, J. J. CRISPR-Based Diagnostics. *Nat. Biomed. Eng.* **2021**, *5* (7), 643–656.
(27) Newsham, E.; Richards-Kortum, R. CRISPR-Based Electrochemical Sensor Permits Sensitive and Specific Viral Detection in Low-Resource Settings. *ACS Cent. Sci.* **2021**, *7* (6), 926–928.
(28) Bruch, R.; Baaske, J.; Chatelle, C.; Meirich, M.; Madlener, S.; Weber, W.; Dincer, C.; Urban, G. A. CRISPR/Cas13a-Powered Electrochemical Microfluidic Biosensor for Nucleic Acid Amplification-Free miRNA Diagnostics. *Adv. Mater.* **2019**, *31* (51), No. 1905311.
(29) Shi, X.; Hu, C.; Guo, B.; Yang, Z.; Zhou, J.; Wang, Z.; Wang, F. A Toehold Switch Biosensor for Versatile miRNA Imaging and Therapeutic Application in Living Cells and Acute Liver Injury Mouse Models. *ACS Sens.* **2025**, *10* (6), 4454–4466.
(30) Hu, C.; Shi, X.; Guo, B.; Yang, Z.; Zhou, J.; Wang, F. Toehold-Based CRISPR-dCas9 Transcriptional Activation Platform for Spatiotemporally Controllable Gene Therapy in Tumor and Diabetic Mouse Models. *ACS Nano* **2025**, *19* (12), 12277–12287.
(31) Shu, W.-J.; Ma, Z.; Jia, L.; Guo, B.; Tian, X.; He, C.; Wang, F. MiR-ON-CRISPR: A microRNA-Activated CRISPR−dCas9 System for Precise Gene Therapy in Living Cells and Mouse Models of Sepsis. *Nucleic Acids Res.* **2025**, *53* (19), No. gkaf1037.
(32) Huang, W.; Wang, J.; Wang, C.; Liu, Y.; Li, W.; Chen, Q.; Zhai, J.; Xiang, Z.; Liu, C. Expanding Cas12a Activity Control with an RNA G-Quadruplex at the 5′ End of CRISPR RNA. *Adv. Sci.* **2025**, *12* (7), No. 2411305.
(33) Abudayyeh, O. O.; Gootenberg, J. S. CRISPR Diagnostics. *Science* **2021**, *372* (6545), 914–915.
(34) Chen, J. S.; Ma, E.; Harrington, L. B.; Da Costa, M.; Tian, X.; Palefsky, J. M.; Doudna, J. A. CRISPR-Cas12a target binding unleashes indiscriminate single-stranded DNase activity. *Science* **2018**, *360* (6387), 436–439.
(35) Rossetti, M.; Merlo, R.; Bagheri, N.; Moscone, D.; Valenti, A.; Saha, A.; Arantes, P. R.; Ippodrino, R.; Ricci, F.; Treglia, I.; Delibato, E.; van der Oost, J.; Palermo, G.; Perugino, G.; Porchetta, A. Enhancement of CRISPR/Cas12a Trans-Cleavage Activity Using Hairpin DNA Reporters. *Nucleic Acids Res.* **2022**, *50* (14), 8377–8391.
(36) Del Giovane, S.; Bagheri, N.; Di Pede, A. C.; Chamorro, A.; Ranallo, S.; Migliorelli, D.; Burr, L.; Paoletti, S.; Altug, H.; Porchetta, A. Challenges and Perspectives of CRISPR-Based Technology for Diagnostic Applications. *TrAC, Trends Anal. Chem.* **2024**, *172*, No. 117594.
(37) Bagheri, N.; Chamorro, A.; Idili, A.; Porchetta, A. PAM-Engineered Toehold Switches as Input-Responsive Activators of CRISPR-Cas12a for Sensing Applications. *Angew. Chem., Int. Ed.* **2024**, *136* (17), No. e202319677.
(38) Tang, Y.; Song, T.; Gao, L.; Yin, S.; Ma, M.; Tan, Y.; Wu, L.; Yang, Y.; Wang, Y.; Lin, T.; Li, F. A CRISPR-Based Ultrasensitive Assay Detects Attomolar Concentrations of SARS-CoV-2 Antibodies in Clinical Samples. *Nat. Commun.* **2022**, *13* (1), 4667.
(39) Xiong, Y.; Zhang, J.; Yang, Z.; Mou, Q.; Ma, Y.; Xiong, Y.; Lu, Y. Functional DNA Regulated CRISPR-Cas12a Sensors for Point-of-Care Diagnostics of Non-Nucleic-Acid Targets. *J. Am. Chem. Soc.* **2020**, *142* (1), 207–213.
(40) Cheng, X.; Li, Y.; Kou, J.; Liao, D.; Zhang, W.; Yin, L.; Man, S.; Ma, L. Novel non-nucleic acid targets detection strategies based on CRISPR/Cas toolboxes: A review. *Biosens. Bioelectron.* **2022**, *215*, No. 114559.
(41) Liang, M.; Li, Z.; Wang, W.; Liu, J.; Liu, L.; Zhu, G.; Karthik, L.; Wang, M.; Wang, K.- F.; Wang, Z.; Yu, J.; Shuai, Y.; Yu, J.; Zhang, L.; Yang, Z.; Li, C.; Zhang, Q.; Shi, T.; Zhou, L.; Xie, F.; Dai, H.; Liu, X.; Zhang, J.; Liu, G.; Zhuo, Y.; Zhang, B.; Liu, C.; Li, S.; Xia, X.; Tong, Y.; Liu, Y.; Alterovitz, G.; Tan, G. Y.; Li-Xin Zhang, L. X. A CRISPR-Cas12a-derived biosensing platform for the highly sensitive detection of diverse small molecules. *Nat. Commun.* **2019**, *10* (1), 3672.
(42) Wang, K.; Liu, S.; Zhou, S.; Qileng, A.; Wang, D.; Liu, Y.; Chen, C.; Lei, C.; Nie, Z. Ligand-Responsive Artificial Protein−Protein Communication for Field-Deployable Cell-Free Biosensing. *Angew. Chem., Int. Ed.* **2025**, *137* (4), No. e202416671.
(43) Chin, L.; Gray, J. W. Translating Insights from the Cancer Genome into Clinical Practice. *Nature* **2008**, *452* (7187), 553–563.
(44) Paz-Elizur, T.; Elinger, D.; Leitner-Dagan, Y.; Blumenstein, S.; Krupsky, M.; Berrebi, A.; Schechtman, E.; Livneh, Z. Development of an Enzymatic DNA Repair Assay for Molecular Epidemiology Studies: Distribution of OGG Activity in Healthy Individuals. *DNA Repair* **2007**, *6* (1), 45–60.
(45) Collins, A. R. The Comet Assay for DNA Damage and Repair. *Mol. Biotechnol.* **2004**, *26* (3), 249–261.
(46) Nagel, Z. D.; Margulies, C. M.; Chaim, I. A.; McRee, S. K.; Mazzucato, P.; Ahmad, A.; Abo, R. P.; Butty, V. L.; Forget, A. L.; Samson, L. D. Multiplexed DNA Repair Assays for Multiple Lesions and Multiple Doses via Transcription Inhibition and Transcriptional

Downloaded from pubs.acs.org/asce/article-pdf/11/2/1634/6486845/se-2025-041187.pdf by guest on 02 September 2026

Mutagenesis. *Proc. Natl. Acad. Sci. U. S. A.* **2014**, *111* (18), E1823–E1832.
(47) O'Connor, M. J. Targeting the DNA Damage Response in Cancer: Molecular Cell. *Mol. Cell* **2015**, *60* (4), 547–560.
(48) Curtin, N. J. DNA Repair Dysregulation from Cancer Driver to Therapeutic Target. *Nat. Rev. Cancer* **2012**, *12* (12), 801–817.
(49) Wilson, D. L.; Kool, E. T. Fluorescent Probes of DNA Repair. *ACS Chem. Biol.* **2017**, *13* (7), 1721–1733.
(50) Luan, X.; Tang, X.; Deng, J.; Yang, Y.; Zhai, J.; Luan, T. Fluorescent Nucleic Acid Probes for DNA Repair Enzymes: Design Strategies and Applications. *TrAC, Trends Anal. Chem.* **2024**, *171*, No. 117489.
(51) Jun, Y. W.; Albarran, E.; Wilson, D. L.; Ding, J.; Kool, E. T. Fluorescence Imaging of Mitochondrial DNA Base Excision Repair Reveals Dynamics of Oxidative Stress Responses. *Angew. Chem., Int. Ed.* **2022**, *134* (6), No. e202111829.
(52) Jun, Y. W.; Kool, E. T. Chemical Tools for the Study of DNA Repair | Accounts of Chemical Research. *Acc. Chem. Res.* **2022**, *55* (23), 3495–3506.
(53) Hu, M.; Cheng, X.; Wu, T. Modular CRISPR/Cas12a Synergistic Activation Platform for Detection and Logic Operations. *Nucleic Acids Res.* **2024**, *52* (12), 7384–7396.
(54) Yin, N.; Yu, H.; Zhang, L.; Luo, F.; Wang, W.; Han, X.; He, Y.; Zhang, Y.; Wu, Y.; Pu, J.; Feng, T.; Yang, G.; Chen, T.; Xie, G. Regulation of CRISPR Trans-Cleavage Activity by an Overhanging Activator. *Nucleic Acids Res.* **2025**, *53* (4), No. gkaf117.
(55) Wu, Y.; Lv, B.; He, T.; Li, D. Alkaline Phosphatase-Assisted Flap Engineering in CRISPR/Cas12a for Biosensing Applications. *Chem. Eng. J.* **2025**, *525*, No. 170484.
(56) Kang, W.; Xiao, F.; Zhu, X.; Ling, X.; Xie, S.; Li, R.; Yu, P.; Cao, L.; Lei, C.; Qiu, Y.; Liu, T.; Nie, Z. Engineering Anti-CRISPR Proteins to Create CRISPR-Cas Protein Switches for Activatable Genome Editing and Viral Protease Detection. *Angew. Chem., Int. Ed.* **2024**, *136* (16), No. e202400599.
(57) Di Pede, A. C.; Bagheri, N.; Belforte, E.; Palone, A.; Rossetti, M.; Porchetta, A. Triplex DNA Clamp Regulates Cas12a Activation for ssDNA and RNA Sensing. *Nucleic Acids Res.* **2026**, *54* (1), No. gkaf1392.
(58) Li, X.; Zhu, Z.; Wu, J.; Li, C.; Liu, Z.; Wang, J.; Li, P.; Zhang, Z.; Huang, Y.; Hong, J.; Wu, T. PAM-Free Hairpin Target Binding Activates Trans-Cleavage Activity of Cas12a. *Nucleic Acids Res.* **2025**, *53* (12), No. gkaf596.
(59) Savva, R.; McAuley-Hecht, K.; Brown, T.; Pearl, L. The structural basis of specific base-excision repair by uracil–DNA glycosylase. *Nature* **1995**, *373* (6514), 487–493.
(60) Weeks, L. D.; Fu, P.; Gerson, S. L. Uracil–DNA Glycosylase Expression Determines Human Lung Cancer Cell Sensitivity to Pemetrexed. *Mol. Cancer Ther.* **2013**, *12* (10), 2248–2260.
(61) Nilsen, H.; Stamp, G.; Andersen, S.; Hrivnak, G.; Krokan, H. E.; Lindahl, T.; Barnes, D. E. Gene-Targeted Mice Lacking the Ung Uracil-DNA Glycosylase Develop B-Cell Lymphomas. *Oncogene* **2003**, *22* (35), 5381–5386.
(62) Swarts, D. C.; Jinek, M. Mechanistic Insights into the *Cis*- and *Trans*-Acting DNase Activities of Cas12a. *Mol. Cell* **2019**, *73* (3), 589–600.
(63) Chen, X.; Wu, Y.; Cao, G.; Wang, X.; Ji, Z.; Huo, D.; Xu, F.; Hou, C. A Methodology for Ultrasensitive Detection of Sequence-Specific DNA or Uracil-DNA Glycosylase Activity. *ACS Sens.* **2020**, *5* (6), 1615–1623.
(64) Du, Y.-C.; Wang, S.-Y.; Wang, Y.-X.; Ma, J.-Y.; Wang, D.-X.; Tang, A.-N.; Kong, D.-M. Terminal Deoxynucleotidyl Transferase Combined CRISPR-Cas12a Amplification Strategy for Ultrasensitive Detection of Uracil-DNA Glycosylase with Zero Background. *Biosens. Bioelectron.* **2021**, *171*, No. 112734.
(65) Dong, K.; Shu, W.; Zhang, J.; Cheng, S.; Zhang, J.; Zhao, R.; Hua, T.; Zhang, W.; Wang, H. Ultra-Sensitive Biosensor Based on CRISPR-Cas12a and Endo IV Coupled DNA Hybridization Reaction for Uracil DNA Glycosylase Detection and Intracellular Imaging. *Biosens. Bioelectron.* **2023**, *226*, No. 115118.
(66) Li, Y.; Yang, X.; Dong, Y.; Wang, J.; Liu, C. CRISPR–Cas12a Detection of DNA Glycosylases via DNA Modification Switching. *Chem. Commun.* **2024**, *60* (86), 12569–12572.
(67) Wang, J.; Zhang, W.; Li, W.; Xie, Q.; Zang, Z.; Liu, C. Enhancement of CRISPR-Cas12a System through Universal Circular RNA Design. *Cell Rep. Methods* **2025**, *5* (6), No. 101076.
(68) Zhang, W.; Zhong, Y.; Wang, J.; Zou, G.; Chen, Q.; Liu, C. Direct Repeat Region 3′ End Modifications Regulate Cas12a Activity and Expand Its Applications. *Nucleic Acids Res.* **2025**, *53* (3), No. gkaf040.
(69) Guo, B.; Hu, C.; Yang, Z.; Tang, C.; Zhang, C.; Wang, F. Test Strip Coupled Cas12a-Assisted Signal Amplification Strategy for Sensitive Detection of Uracil-DNA Glycosylase. *Lab Chip* **2024**, *24* (7), 1987–1995.
(70) Cui, C.; Chen, T.-H. CRISPR/Cas12a Trans-Cleavage Triggered by Cleavage Ligation of Dumbbell DNA for Specific Detection of Human 8-Oxoguanine DNA Glycosylase Activity. *Microchim. Acta* **2023**, *190* (12), 468.
(71) Schormann, N.; Ricciardi, R.; Chattopadhyay, D. Uracil-DNA Glycosylases—Structural and Functional Perspectives on an Essential Family of DNA Repair Enzymes. *Protein Sci.* **2014**, *23* (12), 1667–1685.
(72) Krokan, H. E.; Standal, R.; Slupphaug, G. DNA Glycosylases in the Base Excision Repair of DNA. *Biochem. J.* **1997**, *325* (1), 1–16.
(73) Kuznetsova, A. A.; Kuznetsov, N. A.; Ishchenko, A. A.; Saparbaev, M. K.; Fedorova, O. S. Step-by-Step Mechanism of DNA Damage Recognition by Human 8-Oxoguanine DNA Glycosylase. *Biochim. Biophys. Acta Gen. Subj.* **2014**, *1840* (1), 387–395.
(74) Shinmura, K.; Kasai, H.; Sasaki, A.; Sugimura, H.; Yokota, J. 8-Hydroxyguanine (7,8-Dihydro-8-Oxoguanine) DNA Glycosylase and AP Lyase Activities of hOGG1 Protein and Their Substrate Specificity. *Mutat. Res./DNA Repair* **1997**, *385* (1), 75–82.
(75) Le Marchand, L.; Donlon, T.; Lum-Jones, A.; Seifried, A.; Wilkens, L. R. Association of the hOGG1 Ser326Cys Polymorphism with Lung Cancer Risk1. *Cancer Epidemiol., Biomarkers Prev.* **2002**, *11* (4), 409–412.
(76) Xu, J.; Zheng, S. L.; Turner, A.; Isaacs, S. D.; Wiley, K. E.; Hawkins, G. A.; Chang, B.; Bleecker, E. R.; Walsh, P. C.; Meyers, D. A.; Isaacs, W. B. Associations between hOGG1 Sequence Variants and Prostate Cancer Susceptibility. *Cancer Res.* **2002**, *62* (8), 2253–2257.
(77) Fukae, J.; Takanashi, M.; Kubo, S.; Nishioka, K.; Nakabeppu, Y.; Mori, H.; Mizuno, Y.; Hattori, N. Expression of 8-Oxoguanine DNA Glycosylase (OGG1) in Parkinson's Disease and Related Neurodegenerative Disorders. *Acta Neuropathol.* **2005**, *109* (3), 256–262.
(78) Chen, S.-K.; Hsieh, W. A.; Tsai, M.-H.; Chen, C.-C.; Hong, A.Ic.; Wei, Y.-H.; Chang, W. P. Age-Associated Decrease of Oxidative Repair Enzymes, Human 8-Oxoguanine DNA Glycosylases (hOgg1), in Human Aging. *J. Radiat. Res.* **2003**, *44* (1), 31–35.
(79) Hamm, M. L.; Gill, T. J.; Nicolson, S. C.; Summers, M. R. Substrate Specificity of Fpg (MutM) and hOGG1, Two Repair Glycosylases. *J. Am. Chem. Soc.* **2007**, *129* (25), 7724–7725.
(80) Visnes, T.; Cázares-Körner, A.; Hao, W.; Wallner, O.; Masuyer, G.; Loseva, O.; Mortusewicz, O.; Wiita, E.; Sarno, A.; Manoilov, A.; Astorga-Wells, J.; Jemth, A.-S.; Pan, L.; Sanjiv, K.; Karsten, S.; Gokturk, C.; Grube, M.; Homan, E. J.; Hanna, B. M. F.; Paulin, C. B. J.; Pham, T.; Rasti, A.; Berglund, U. W.; von Nicolai, C.; Benitez-Buelga, C.; Koolmeister, T.; Ivanic, D.; Iliev, P.; Scobie, M.; Krokan, H. E.; Baranczewski, P.; Artursson, P.; Altun, M.; Jensen, A. J.; Kalderén, C.; Ba, X.; Zubarev, R. A.; Stenmark, P.; Boldogh, I.; Helleday, T. Small-Molecule Inhibitor of OGG1 Suppresses Proinflammatory Gene Expression and Inflammation. *Science* **2018**, *362* (6416), 834–839.
(81) Visnes, T.; Benítez-Buelga, C.; Cázares-Körner, A.; Sanjiv, K.; Hanna, B. M. F.; Mortusewicz, O.; Rajagopal, V.; Albers, J. J.; Hagey, D. W.; Bekkhus, T.; Eshtad, S.; Baquero, J. M.; Masuyer, G.; Wallner, O.; Müller, S.; Pham, T.; Göktürk, C.; Rasti, A.; Suman, S.; Torres-Ruiz, R.; Sarno, A.; Wiita, E.; Homan, E. J.; Karsten, S.; Marimuthu, K.; Michel, M.; Koolmeister, T.; Scobie, M.; Loseva, O.; Almlöf, I.;

Downloaded from pubs.acs.org/asce/article-pdf/11/2/1634/6486845/se-2025-041187.pdf by guest on 02 September 2026

https://doi.org/10.1021/acssensors.5c04118
ACS Sens. 2026, 11, 1634–1644

Unterlass, J. E.; Pettke, A.; Boström, J.; Pandey, M.; Gad, H.; Herr, P.; Jemth, A.-S.; El Andaloussi, S.; Kalderén, C.; Rodriguez-Perales, S.; Benítez, J.; Krokan, H. E.; Altun, M.; Stenmark, P.; Berglund, U. W.; Helleday, T. Targeting OGG1 Arrests Cancer Cell Proliferation by Inducing Replication Stress. *Nucleic Acids Res.* **2020**, *48* (21), 12234–12251.

(82) Donley, N.; Jaruga, P.; Coskun, E.; Dizdaroglu, M.; McCullough, A. K.; Lloyd, R. S. Small Molecule Inhibitors of 8-Oxoguanine DNA Glycosylase-1 (OGG1). *ACS Chem. Biol.* **2015**, *10* (10), 2334–2343.

(83) Tahara, Y.; Auld, D.; Ji, D.; Beharry, A. A.; Kietrys, A. M.; Wilson, D. L.; Jimenez, M.; King, D.; Nguyen, Z.; Kool, E. T. Potent and Selective Inhibitors of 8-Oxoguanine DNA Glycosylase. *J. Am. Chem. Soc.* **2018**, *140* (6), 2105–2114.

(84) Biela, A.; Coste, F.; Culard, F.; Guerin, M.; Goffinont, S.; Gasteiger, K.; Cieśla, J.; Winczura, A.; Kazimierczuk, Z.; Gasparutto, D.; Carell, T.; Tudek, B.; Castaing, B. Zinc Finger Oxidation of Fpg/Nei DNA Glycosylases by 2-Thioxanthine: Biochemical and X-Ray Structural Characterization. *Nucleic Acids Res.* **2014**, *42* (16), 10748–10761.

(85) Rieux, C.; Goffinont, S.; Coste, F.; Tber, Z.; Cros, J.; Roy, V.; Guérin, M.; Gaudon, V.; Bourg, S.; Biela, A.; Aucagne, V. Thiopurine Derivative-Induced Fpg/Nei DNA Glycosylase Inhibition: Structural, Dynamic and Functional Insights. *Int. J. Mol. Sci.* **2020**, *21* (6), No. 2058.

(86) Loock, H.-P.; Wentzell, P. D. Detection Limits of Chemical Sensors: Applications and Misapplications. *Sens. Actuators, B* **2012**, *173*, 157–163.

Downloaded from pubs.acs.org/ascef/article-pdf/11/2/1634/6486845/se-2025-041187.pdf by guest on 02 September 2026

https://doi.org/10.1021/acssensors.5c04118
ACS Sens. 2026, 11, 1634–1644